Review Article

PMP

Progress in Medical Physics 28(4), December 2017
https://doi.org/10.14316/pmp.2017.28.4.135
pISSN 2508-4445, eISSN 2508-4453

Physical Modeling of Chemical Exchange Saturation Transfer Imaging

Geon-Ho Jahng*, Jang-Hoon Oh†

*Department of Radiology, Kyung Hee University Hospital at Gangdong, College of Medicine, Kyung Hee University,
†Department of Radiology, Kyung Hee University Hospital, Kyung Hee University, Seoul, Korea

Received 13 November 2017
Revised 18 December 2017
Accepted 19 December 2017

Corresponding author
Geon-Ho Jahng
(ghjahng@gmail.com)
Tel: 82-2-440-6187
Fax: 82-2-440-6932

Chemical Exchange Saturation Transfer (CEST) imaging is a method to detect solutes based on the chemical exchange of mobile protons with water. The solute protons exchange with three different patterns, which are fast, slow, and intermediate rates. The CEST contrast can be obtained from the exchangeable protons, which are hydroxyl protons, amine protons, and amide protons. The CEST MR imaging is useful to evaluate tumors, strokes, and other diseases. The purpose of this study is to review the mathematical model for CEST imaging and for measurement of the chemical exchange rate, and to measure the chemical exchange rate using a 3T MRI system on several amino acids. We reviewed the mathematical models for the proton exchange. Several physical models are proposed to demonstrate a two-pool, three-pool, and four-pool models. The CEST signals are also evaluated by taking account of the exchange rate, pH and the saturation efficiency. Although researchers have used most commonly in the calculation of CEST asymmetry, a quantitative analysis is also developed by using Lorentzian fitting. The chemical exchange rate was measured in the phantoms made of asparagine (Asn), glutamate (Glu), γ-aminobutyric acid (GABA), glycine (Gly), and myoinositol (MI). The experiment was performed at a 3T human MRI system with three different acidity conditions (pH 5.6, 6.2, and 7.4) at a concentration of 50 mM. To identify the chemical exchange rate, the "lsqcurvefit" built-in function in MATLAB was used to fit the pseudo-first exchange rate model. The pseudo-first exchange rate of Asn and Gly was increased with decreasing acidity. In the case of GABA, the largest result was observed at pH 6.2. For Glu, the results at pH 5.6 and 6.2 did not show a significant difference, and the results at pH 7.4 were almost zero. For MI, there was no significant difference at pH 5.6 or 7.4, however, the results at pH 6.2 were smaller than at the other pH values. For the experiment at 3T, we were only able to apply 1 s as the maximum saturation duration due to the limitations of the MRI system. The measurement of the chemical exchange rate was limited in a clinical 3T MRI system because of a hardware limitation.

Keywords: CEST, physical model, exchange rate, 3T human MRI

Principle of CEST Imaging

Chemical Exchange Saturation Transfer (CEST) imaging is a method to detect solutes based on the chemical exchange of mobile protons with water[1,2] The reversible exchange of protons between two molecules is separated by a chemical shift frequency (Δf) and governed by a single reaction rate (k) which can vary from nanoseconds to many seconds, depending on the system interested.[3] If the exchange rate is slow on the chemical shift time scale ($k<<\Delta f$), two-split sets of signals are observed. For fast exchange rates ($k>>\Delta f$) only one peak signal is observed

at an average frequency corresponding to the relative populations of the two chemical species. At intermediate exchange rates ($k \approx \Delta f$) very large spectral line widths, corresponding to very short T2 values, occur.[4] One of the strong *in-vivo* contributions to CEST contrast are hydroxyl protons at approximately l ppm above water, that have been used to assess glycogen (Glyco) CEST,[5] glycosaminoglycans (GAG) CEST,[6] Glucose (Gluco) CEST,[7] and Myoinositol (MI) CEST.[8,9] These molecules in tissues dominate rapidly exchanging hydroxyl protons and therefore it is difficult to measure CEST signals with a commercial 3T MRI system. Another strong in-vivo contribution to the CEST contrast is amine protons at amine protons of amino acids and other molecules between 2–3 ppm above water, that have been used to assess Glutamate (Glu) CEST,[9,10] γ-Aminobutyric Acid (GABA) CEST,[9,11] Glycine CEST,[9] and Creatine (Cr) CEST.[12] he amine protons have intermediate exchange rates and therefore a high magnetic field system is beneficial to obtain its signals. Finally, most common target protons are amide protons at approximately 3.5 ppm, which are dominantly existed the backbone of proteins, have a larger chemical shift, and have the more slowly exchanging. Because amide protons permit saturation at low power levels, amide proton transfer (APT) imaging is particularly attractive for endogenous CEST contrast in human applications.[13,14] The purpose of this study is to review the mathematical model for CEST imaging and for measurement of the chemical exchange rate and to measure the chemical exchange rate using a 3T MRI system on several amino acids.

Modeling of Chemical Exchange Proton Transfer Imaging

1. Two-site exchange modeling for CEST imaging

CEST processes can be described by a two-pool exchange model, which has small and large pools. The small pool (s) represents the exchangeable solute protons and the large pool (w) does bulk water protons. In the pools, we can define the following parameters: M_{0s} and M_{0w} are the equilibrium magnetization for the solute pool and the water pool, respectively. ω_{0s} and ω_{ow} are the resonance frequencies of the exchangeable solute proton and of the water pool, respectively. T_{1s} and T_{2s} as well as T_{1w} and T_{2w} are the longitudinal and transverse relaxation rates for the solute protons and the water protons, respectively. Finally, k_{sw} and k_{ws} are the exchange rates of magnetization from pool (s) to pool (w) and vice versa. The MR signal for the two exchanging pools is modeled by modified Bloch equations including exchange terms.[15,16] Under the equilibrium condition, the system obeys the relationship $k_{sw}*M_{Os}=k_{ws}*M_{ow}$. In the weak saturation approximation, it is assumed that the RF irradiation is applied on resonance with the solute pool (s) while leaving the water pool (w) unperturbed (no direct water saturation).[16,17] Therefore, (ω_{os}, -ω) is zero and (ω_{0w}, -ω) approaches infinite.

1) Steady state condition

The Bloch equations can be simplified to four equations with exact steady state analytical solutions. The steady state (ss) longitudinal magnetization (M_z) for the water and the solute pools under the weak saturation approximation are[16,17]:

$$\frac{M_{zw,ss}}{M_{ow}} = 1 - \left(\frac{M_{os}}{M_{ow}}\right)\left(\frac{\propto k_{sw}}{R_{1w} + k_{ws}}\right) \quad [1]$$

$$\frac{M_{zs,ss}}{M_{os}} = 1 - \alpha \quad [2]$$

Where α is the saturation efficiency and depends on the relaxation times T_1 and T_2 as well as the pool-to-pool exchange rates.

2) Time dependent condition

The time dependent solution can be obtained in the weak saturation approximation by separating the saturation process of pool (s) and transfer to pool (w) into two separate steps.[16,17] Assuming that pool (s) approaches the steady state $M_{zs,ss}$ instantly, the dynamics for pool (w) can be described by

$$M_{zw} = M_{ow} - \left(\frac{k_{sw} \propto M_{0s}}{R_{1w} + k_{ws}}\right)\left[1 - e^{-(R_{1w}+k_{ws})T_{sat}}\right] \quad [3]$$

where T_{sat} is the applied RF saturation duration. Since direct water saturation is assumed to be zero in the weak

saturation approximation, the CEST signal or proton transfer ratio simplifies to $CEST_{weak}$ or $PTR_{weak}=(1-M_{zw}/M_{ow})$. Note that we used the assumption of no direct water saturation in the above solution. To take account for direct water saturation, a different analytical solution can be derived under the assumption of strong saturation pulse. In this review, we do not explain the solution of the Bloch equation. Readers who interest the solution read the references.[18-20] Finally, recently three-pool[21,22] or four-pool[23] exchange models were introduced with separating the exchangeable protons as small solute protons and broad macromolecular protons and with the bulk water protons. Most of the chemical exchange mechanisms result in a field-dependent shortening of both T1 and T2, with typically a much greater effect on T2. Chemical exchanges occurring over time frames longer than T1 do not generally affect spectral lines widths or the MR signal.

2. CEST with the saturation efficiency

A previous study showed the relationship between CEST asymmetry and B1 amplitude.[24] Saturation efficiency, known as α, which express the relationship, is increased with increasing B_1 power in a certain range and is reached a steady-state with a further increased B_1 power. The proton transfer rate (PTR) which represents the CEST asymmetry in the two-poll exchange model is proportional to the saturation efficiency[25] shown in the following equations:

$$\mathrm{PTR} = C_s * \alpha * k_{sw} * T_{1w}\left(1 - e^{-t_{sat}/T_{1w}}\right) \quad [4]$$

$$\alpha \approx \frac{(\gamma B_1)^2}{(\gamma B_1)^2 + (k_{sw})^2} \quad [5]$$

where C_s is the fractional concentration, k_{sw} is the exchange rate, T_{1w} is the longitudinal relaxation rate of water, and t_{sat} is the saturation time. According to Eqs. [4] and [5], the B1 amplitude is related to α. As the exchange rate is constant (k_{sw} is 1), the CEST effect in turn increases with increasing the B1 amplitude. A tendency for the CEST effect is to increase as the B1 amplitude increases. A previous study showed that the saturation efficiency is deceased with the fast exchanging rate.[25]

3. CEST with acidity

The overall CEST contrast is a function of both the solute proton concentration (M_{os}/M_{ow}) and the chemical exchange rate (k_{sw}) of the solute proton with water. The exchange rate is particularly important because it depends on the pH and therefore the CEST effect is strongly dependent on pH. The exchange rate and acidity are complexly related, and defined by the following equation[24]:

$$k_{sw} = k_0 + k_a \times 10^{pH} + k_b \times 10^{pH-pk_w} \quad [6]$$

where k_{sw} is the single-proton solute-water exchange rate, k_0 is the spontaneous exchange, k_a is the acid-catalyzed exchange, k_b is the base-catalyzed exchange, k_w is the ionization constant of water. When the concentration of the molecules remained the same, the number of exchangeable protons also remained the same. When the pH was varied, the exchange rate changed, and therefore the CEST effect was affected by pH. Previous research has demonstrated that the CEST effect of amide and amine groups has a complex relationship with the chemical exchange rate and acidity.[26,27] We previously showed that the CEST asymmetry of the molecules was decreased with increasing pH at 9.4T MRI.[9] The CEST asymmetry values for GABA, Glu, and Gly which contain amine groups were lowest with the highest pH which was consistent with the previous amine group studies,[9,28] which showed the decreased CEST asymmetry values with increasing pH for the amine protons.

4. CEST signal with the exchange rate

The exchange rate and CEST effect are related by the following simple equations[2]:

$$M_s/M_0 \approx \left[1 - k_1 T_{1SAT}\right] \quad [7]$$

$$k_1 = k_{CA}[Agent][n] \quad [8]$$

In which, M_s is the magnitude of the water proton signal during the saturation of the exchangeable protons in the metabolite of interest, M_0 is the magnitude of the signal

under controlled irradiation at the opposite frequency offset, k_1 is the pseudo first-order exchange rate constant, T_{1SAT} is the spin-lattice relaxation time constant of water protons as measured during the saturation of the exchange metabolite, K_{CA} is the single exchange site rate constant (the same as k_{sw}), [Agent] is the mole fraction of the exchanging agent, and [n] is the number of exchange sites.

5. Lorentzian modeling to fit a full Z spectrum

Most of previous studies are used to asymmetry calculations of the full Z spectrum to show CEST contrast. However, the asymmetry value is not quantitative and is relative to opposite frequency for the interested protons. Therefore, researchers are tried to obtain a quantitative value from the full Z spectrum. For modeling of in-vivo full Z spectrum, the Lorentzian line shape fitting method can be used. The following formula can be used for the six pool Lorentzian fitting.[29]

$$Z = Z_{ini} = \sum_{i=1}^{6} \frac{Ai \,.\, \Gamma_i^2/5}{\Gamma_i^2/5 + (\Delta\omega_{RF} - \delta\omega_i)} \quad [9]$$

Where Z_{ini} was each baseline of six pools, Ai is the amplitude of six pools, Γ_i is the full width at half maximum (FWHM) of six pools, $\Delta\omega_{RF}$ is the frequency of Radio frequency and $\delta\omega_i$ is the frequency offset of six pools. Table 1 lists the initial value, the lower limit, and the upper limit of the amplitude, FWHM, and the center frequency of the six pools. The six pool protons are defined in the initial offset frequency values as water at 0 ppm, amide at 3.5 ppm, amine at 3.0 ppm, hydroxyl at 0.9 ppm, the nuclear overhauser effect (NOE) at -3.5 ppm, and the magnetization transfer (MT) at -1.5 ppm.[8,30-32] The problems with this Lorentzian fitting are that the fitted results are strongly depended on the initial values and the calculation takes relatively long time compared to that to obtain the asymmetry value.

6. CEST asymmetry

The most common method to evaluate the CEST data is to calculate the asymmetry value. The frequency-dependent saturation effects are visualized as a signal loss at a specific frequency. The saturation effects are asymmetric with respect to the water resonance frequency, and can be removed by asymmetry analysis, where the water signal from one side of the Z-spectrum is subtracted from the other. The CEST asymmetry ratio ($CEST_{asym}$) is calculated using the following equation[25,33]:

$$CEST_{asym} = \frac{M_{sat}(-\Delta\omega) - M_{sat}(+\Delta\omega)}{M_0} \quad [10]$$

In which $\Delta\omega$ is the frequency difference from water, M_{sat} is the magnetization with the saturation pulse, M_0 is the magnetization observed without saturation. Usually

Table 1. Initial values, the lower limit, and the upper limit of the amplitude, the full width of half maximum (FWHM), and the center frequency of the six pools for Lorentzian curve fitting.

	Initial values	Lower limit	Upper limit
Water			
Amplitude	0.45	0.0	inf
FWHM (ppm)	8.00	0.0	inf
Frequency (ppm)	0	–1.0	1.0
Amine			
Amplitude	0.060	0.0	1
FWHM (ppm)	0.80	0.0	2.6
Frequency (ppm)	2.8	1.80	3.80
Amide			
Amplitude	0.060	0.0	1
FWHM (ppm)	0.80	0.0	2.6
Frequency (ppm)	3.5	2.50	4.50
Hydroxyl			
Amplitude	0.020	0.00	1
FWHM (ppm)	0.2	0.10	1.8
Frequency (ppm)	0.9	0.0	1.8
NOE			
Amplitude	0.020	0.0	1
FWHM (ppm)	2.28	0.0	4.46
Frequency (ppm)	–3.5	–4.5	–2.5
MT			
Amplitude	0.08	0.0	1
FWHM (ppm)	9.04	0.0	inf
Frequency (ppm)	–1.5	–3.5	1.5

The amplitude is no unit because of the normalization of the full Z spectrum signals by the reference signal.
The frequency (ppm) is the center frequency of the exchangeable protons.
The six pool protons were defined in the initial offset frequency values as water at 0 ppm, amide at 3.5 ppm, amine at 3.0 ppm, hydroxyl at 0.9 ppm, the nuclear overhauser effect (NOE) at –3.5 ppm, and the magnetization transfer (MT) at –1.5ppm.

the CEST effect from solute protons is detected over a frequency range less than 6 ppm from water.

Modeling for the Measurement of the Chemical Exchange Rate

1. Experiment to measure the chemical exchange rate

As we mentioned in the previous session, the determination of the chemical exchange rate is important to CEST MRI because CEST signals are depended on this exchange rate. Experiments to measure the chemical exchange rate were performed at the 3T human MRI system (Acheiva, Philips). In order to identify the tendency between the exchange rate and acidity, phantoms were developed by asparagine (Asn), glutamate (Glu), γ-aminobutyric acid (GABA), glycine (Gly), and myoinositol (MI) with three different acidity conditions (pH 5.6, 6.2, and 7.4) at a concentration of 50 mM were used in the experiment. The B_1 amplitude of 3 μT was used. To identify the exchange rate, saturation pulse durations [t_{sat}] of 0, 0.07, 0.21, 0.35, 0.49, 0.63, 0.77, and 0.91 s were used, consisting of a 70 ms saturation pulse multiplied by 0, 1, 3, 5, 7, 9, 11, and 13 pulses per 1 TR, with a 0.8 RF duty cycle. We only used 0.91 s for the maximum duration of each saturation pulse because the clinical MRI system only allowed 1 s of the maximum duration of the saturation pulse.

To identify the chemical exchange rate, the "lsqcurvefit" built-in function in MATLAB was used to fit the pseudo-first exchange rate model, which is Eq. [11][24]:

$$CEST = \frac{(S_{0w} - S_w(t_{sat},\alpha)}{S_{0w}} = \frac{k_{sw} \times \alpha \times X_{CA}}{R_{1w} + k_{sw} \times X_{CA}} \times [1 - e^{-(R_{1w} + k_{sw} \times X_{CA})t_{sat}}] \quad [11]$$

In which S_{0w} and S_w (t_{sat}, α) are the water signals without and with saturation, respectively. t_{sat} and α are the saturation duration and saturation efficiency, respectively. R_{1w} is the longitudinal relaxation rate ($1/T_1$) for water (R_{1w} ~0.248 s^{-1}), X_{CA} is the fractional concentration of exchangeable protons of the CEST agent, and the term $k_{sw} \times X_{ca}$ can be expressed as the pseudo first-order exchange rate constant k_1. In this study, we fitted Eq. [11] to obtain k_1 with assumption of R_{1w}=0.248 s^{-1}) and α=1.

2. Result of measurements of the chemical exchange rate at 3T

The pseudo-first exchange rate of Asn and Gly was increased with decreasing acidity. In the case of GABA, the largest result was observed at pH 6.2. For Glu, the results at pH 5.6 and 6.2 did not show a significant difference, and the results at pH 7.4 were almost zero. For MI, there was no significant difference at pH 5.6 or 7.4, however, the results at pH 6.2 were smaller than at the other pH values. Fig. 1 shows the fitting results of the exchange rate experiments of the five target molecules with different pH values (acidity) at a concentration of 50 mM at 3T. Table 2 lists the fitting results with k_1, and the value of the squared 2-norm of the residual (resnorm). Usually, the amide group has a slow exchange rate,[34] and the CEST effect for the amide protons increases as pH increases because the exchange rate increases in a low pH.[26,27] We showed the pseudo-exchange rates of Glu and Gly were decreased with increasing the acidity.[9] The decreased exchange rate at pH=7.4 can be affected in decreasing the CEST asymmetry for the amine proton.

In Eq [11], k_{sw} and X_{CA} are not MRI scanning conditions or chemical properties, and $k_{sw} \times X_{CA}$ should remain the same without varying the MR main magnet field. The experiment is based on the fact that the CEST effect should reach a steady-state as the saturation duration increases[24] and that CEST asymmetry can be reached at a saturation duration of almost 5 s. However, for the experiment at 3T, we were only able to apply 1 s as the maximum saturation duration due to the limitations of the MRI system. It is difficult to say whether the result at 3T has enough confidence. Furthermore, to fit $k_{sw} \times X_{CA}$, we assumed that the α constant was 1. According to Eq. [11], α can affect the fitting results.[24] However, α has a complex relationship with the exchange rate, and it is hard to calculate the exact α value from this experiment. To identify the exact exchange rate, an additional experiment would need to be performed in order to measure the α value.

Conclusion

CEST imaging is a relatively new MRI contrast to evalu-

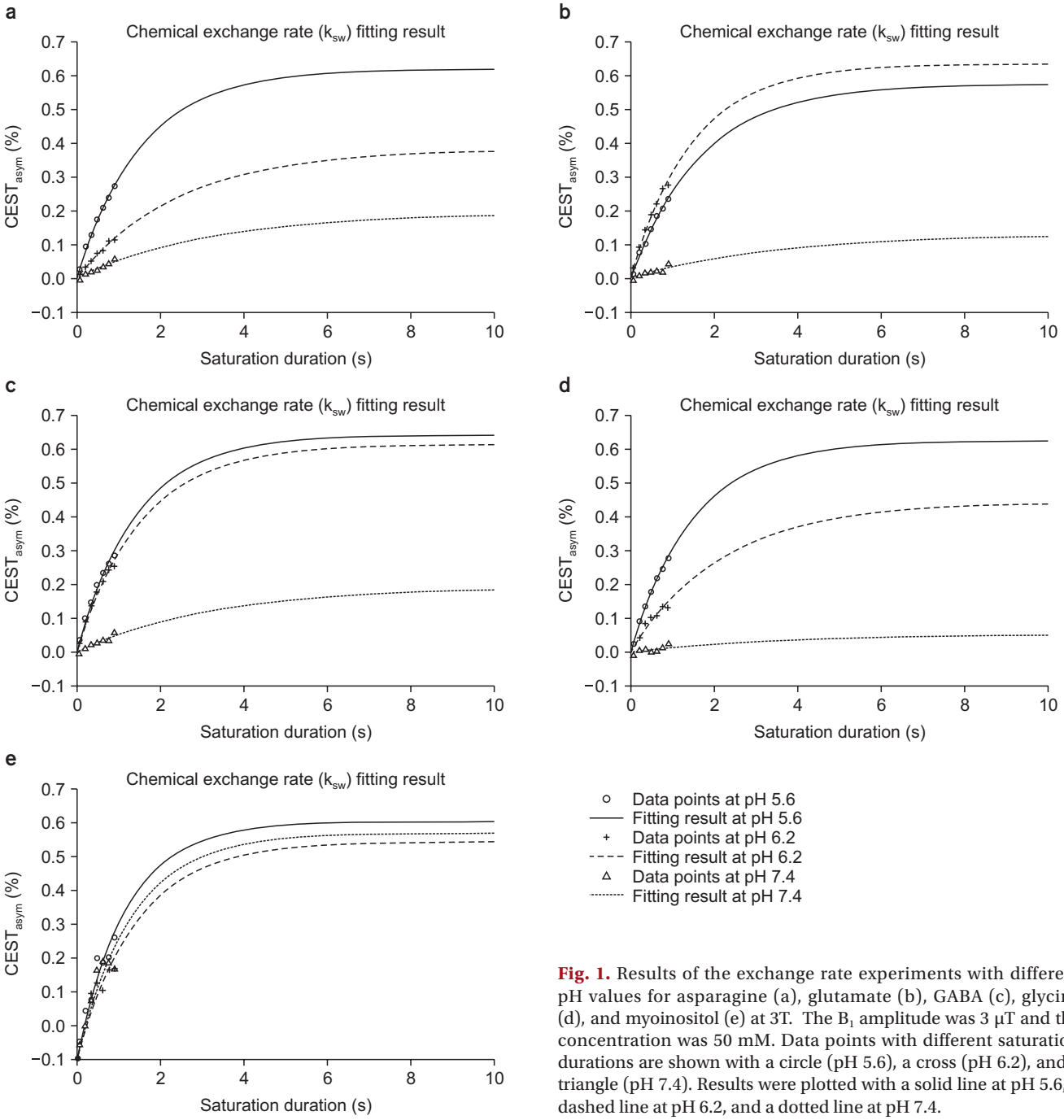

Fig. 1. Results of the exchange rate experiments with different pH values for asparagine (a), glutamate (b), GABA (c), glycine (d), and myoinositol (e) at 3T. The B_1 amplitude was 3 μT and the concentration was 50 mM. Data points with different saturation durations are shown with a circle (pH 5.6), a cross (pH 6.2), and a triangle (pH 7.4). Results were plotted with a solid line at pH 5.6, a dashed line at pH 6.2, and a dotted line at pH 7.4.

ate an endogenous compounds containing in molecules or neurotransmitters. To map the amount of the exchangeable protons, it is necessary to understand the right physical model of the CEST method. Furthermore, the measurement of the chemical exchange rate is key factor to analyze the CEST data. We measured the exchange rate using a 3T MRI system on several amino acids with different conditions of pH, but this measurement was limited in a clinical 3T MRI system because of a hardware limitation.

Acknowledgements

This study was supported by the National Research Foundation of Korea (NRF) grant funded by the Korea

Table 2. Result of the measurement of the pseudo-first exchange rate $k_1=k_{sw}\times X_{ca}$ [s^{-1}] of the 5 target molecules at 3T MRI.

Target molecule	pH	k_1 [s^{-1}]	Resnorm
Asn	pH 5.6	0.4032	0.0003
	pH 6.2	0.1548	0.0001
	pH 7.4	0.0601	0.0002
Glu	pH 5.6	0.4461	0.0007
	pH 6.2	0.3954	0.0007
	pH 7.4	0.0589	0.0003
GABA	pH 5.6	0.3379	0.0003
	pH 6.2	0.4315	0.0005
	pH 7.4	0.0375	0.0003
Gly	pH 5.6	0.4141	0.0002
	pH 6.2	0.1988	0.0009
	pH 7.4	0.0140	0.0004
MI	pH 5.6	0.5898	0.0063
	pH 6.2	0.4482	0.0065
	pH 7.4	0.5025	0.0092

Resnorm, the value of the squared 2-norm of the residual,
The k_1 value was measured at 3.0 ppm for asparagine (Asn), at 2.7 ppm for glutamate (Glu), at 2.7 ppm for γ-aminobutyric acid (GABA) and glycine (Gly), and at 0.9 ppm for myoinositol (MI).

government (MSIP) (2014R1A2A2A01002728) and supported by Basic Science Research Program through the National Research Foundation of Korea (NRF) funded by the Ministry of Education (2016R1D1A1B03930720).

Conflicts of Interest

The authors have nothing to disclose.

Availability of Data and Materials

All relevant data are within the paper and its Supporting Information files.

Ethics Approval and Consent to Participate

The study was approved by the institutional review board (IRB approval number; 2015-02-006-001).

References

1. V. Guivel-Scharen, T. Sinnwell, S.D. Wolff, R.S. Balaban, "Detection of proton chemical exchange between metabolites and water in biological tissues," J Magn Reson 133, 36-45 (1998).
2. K.M. Ward, A.H. Aletras, R.S. Balaban, "A new class of contrast agents for MRI based on proton chemical exchange dependent saturation transfer (CEST)," J Magn Reson 143, 79-87 (2000).
3. O. Millet, J.P. Loria, C.D. Kroenke, M. Pons, A.G. Palmer, "The Static Magnetic Field Dependence of Chemical Exchange Linebroadening Defines the NMR Chemical Shift Time Scale," Journal of the American Chemical Society 122, 2867-2877 (2000).
4. R.G. Spencer, K.W. Fishbein, "Measurement of spin-lattice relaxation times and concentrations in systems with chemical exchange using the one-pulse sequence: breakdown of the Ernst model for partial saturation in nuclear magnetic resonance spectroscopy," J Magn Reson 142, 120-135 (2000).
5. P.C. van Zijl, C.K. Jones, J. Ren, C.R. Malloy, A.D. Sherry, "MRI detection of glycogen in vivo by using chemical exchange saturation transfer imaging (glycoCEST)," Proc Natl Acad Sci U S A 104, 4359-4364 (2007).
6. W. Ling, R.R. Regatte, G. Navon, A. Jerschow, "Assessment of glycosaminoglycan concentration in vivo by chemical exchange-dependent saturation transfer (gagCEST)," Proc Natl Acad Sci U S A 105, 2266-2270 (2008).
7. S. Walker-Samuel, R. Ramasawmy, F. Torrealdea, M. Rega, V. Rajkumar, S.P. Johnson, S. Richardson, M. Goncalves, H.G. Parkes, E. Arstad, D.L. Thomas, R.B. Pedley, M.F. Lythgoe, X. Golay, "In vivo imaging of glucose uptake and metabolism in tumors," Nat Med 19, 1067-1072 (2013).
8. M. Haris, K. Cai, A. Singh, H. Hariharan, R. Reddy, "In vivo mapping of brain myo-inositol," Neuroimage 54, 2079-2085 (2011).
9. J.-H. Oh, H.-G. Kim, D.-C. Woo, H.-K. Jeong, S.Y. Lee, G.-H. Jahng, "Chemical-exchange-saturation-transfer magnetic resonance imaging to map gamma-aminobutyric acid, glutamate, myoinositol, glycine, and asparagine: Phantom experiments," Journal of the Korean Physical Society 70, 545-553 (2017).
10. M. Haris, K. Nath, K. Cai, A. Singh, R. Crescenzi, F. Kogan, G. Verma, S. Reddy, H. Hariharan, E.R. Melhem, R. Reddy, "Imaging of glutamate neurotransmitter alterations in Alzheimer's disease," NMR Biomed 26, 386-391 (2013).
11. G. Yan, T. Zhang, Z. Dai, M. Yi, Y. Jia, T. Nie, H. Zhang, G.

Xiao, R. Wu, "A Potential Magnetic Resonance Imaging Technique Based on Chemical Exchange Saturation Transfer for In Vivo gamma-Aminobutyric Acid Imaging," PLoS One 11, e0163765 (2016).

12. F. Kogan, M. Haris, A. Singh, K. Cai, C. Debrosse, R.P. Nanga, H. Hariharan, R. Reddy, "Method for high-resolution imaging of creatine in vivo using chemical exchange saturation transfer," Magn Reson Med 71, 164-172 (2014).
13. P.C. van Zijl, J. Zhou, N. Mori, J.F. Payen, D. Wilson, S. Mori, "Mechanism of magnetization transfer during on-resonance water saturation. A new approach to detect mobile proteins, peptides, and lipids," Magn Reson Med 49, 440-449 (2003).
14. J. Zhou, J.F. Payen, D.A. Wilson, R.J. Traystman, P.C. van Zijl, "Using the amide proton signals of intracellular proteins and peptides to detect pH effects in MRI," Nat Med 9, 1085-1090 (2003).
15. H.M. McConnell, "Reaction Rates by Nuclear Magnetic Resonance," The Journal of Chemical Physics 28, 430-431 (1958).
16. J. Zhou, D.A. Wilson, P.Z. Sun, J.A. Klaus, P.C. Van Zijl, "Quantitative description of proton exchange processes between water and endogenous and exogenous agents for WEX, CEST, and APT experiments," Magn Reson Med 51, 945-952 (2004).
17. J. Zhou, P. van zijl, Chemical exchange saturation transfer imaging and spectroscopy. (2006).
18. E. Baguet, C. Roby, "Fast Inversion-Recovery Measurements in the Presence of a Saturating Field for a Two-Spin System in Chemical Exchange," Journal of Magnetic Resonance, Series A 108, 189-195 (1994).
19. E. Baguet, C. Roby, "Off-resonance irradiation effect in steady-state NMR saturation transfer," J Magn Reson 128, 149-160 (1997).
20. P.Z. Sun, P.C. van Zijl, J. Zhou, "Optimization of the irradiation power in chemical exchange dependent saturation transfer experiments," J Magn Reson 175, 193-200 (2005).
21. D.E. Woessner, S. Zhang, M.E. Merritt, A.D. Sherry, "Numerical solution of the Bloch equations provides insights into the optimum design of PARACEST agents for MRI," Magn Reson Med 53, 790-799 (2005).
22. K.L. Desmond, G.J. Stanisz, "Understanding quantitative pulsed CEST in the presence of MT," Magn Reson Med 67, 979-990 (2012).
23. A.X. Li, R.H. Hudson, J.W. Barrett, C.K. Jones, S.H. Pasternak, R. Bartha, "Four-pool modeling of proton exchange processes in biological systems in the presence of MRI-paramagnetic chemical exchange saturation transfer (PARACEST) agents," Magn Reson Med 60, 1197-1206 (2008).
24. M.T. McMahon, A.A. Gilad, J. Zhou, P.Z. Sun, J.W. Bulte, P.C. van Zijl, "Quantifying exchange rates in chemical exchange saturation transfer agents using the saturation time and saturation power dependencies of the magnetization transfer effect on the magnetic resonance imaging signal (QUEST and QUESP): Ph calibration for poly-L-lysine and a starburst dendrimer," Magn Reson Med 55, 836-847 (2006).
25. P.C. van Zijl, N.N. Yadav, "Chemical exchange saturation transfer (CEST): what is in a name and what isn't?," Magn Reson Med 65, 927-948 (2011).
26. K.M. Ward, R.S. Balaban, "Determination of pH using water protons and chemical exchange dependent saturation transfer (CEST)," Magn Reson Med 44, 799-802 (2000).
27. X. Zong, P. Wang, S.G. Kim, T. Jin, "Sensitivity and source of amine-proton exchange and amide-proton transfer magnetic resonance imaging in cerebral ischemia," Magn Reson Med 71, 118-132 (2014).
28. N. McVicar, A.X. Li, D.F. Goncalves, M. Bellyou, S.O. Meakin, M.A. Prado, R. Bartha, "Quantitative tissue pH measurement during cerebral ischemia using amine and amide concentration-independent detection (AACID) with MRI," J Cereb Blood Flow Metab 34, 690-698 (2014).
29. M. Zaiss, B. Schmitt, P. Bachert, "Quantitative separation of CEST effect from magnetization transfer and spillover effects by Lorentzian-line-fit analysis of z-spectra," J Magn Reson 211, 149-155 (2011).
30. S. Goerke, M. Zaiss, P. Kunz, K.D. Klika, J.D. Windschuh, A. Mogk, B. Bukau, M.E. Ladd, P. Bachert, "Signature of protein unfolding in chemical exchange saturation transfer imaging," NMR Biomed 28, 906-913 (2015).
31. K.L. Desmond, F. Moosvi, G.J. Stanisz, "Mapping of amide, amine, and aliphatic peaks in the CEST spectra of murine

xenografts at 7 T," Magn Reson Med 71, 1841-1853 (2014).
32. D. Liu, J. Zhou, R. Xue, Z. Zuo, J. An, D.J. Wang, "Quantitative characterization of nuclear overhauser enhancement and amide proton transfer effects in the human brain at 7 tesla," Magn Reson Med 70, 1070-1081 (2013).
33. R.G. Bryant, "The dynamics of water-protein interactions," Annu Rev Biophys Biomol Struct 25, 29-53 (1996).
34. M. Zaiss, P. Bachert, "Chemical exchange saturation transfer (CEST) and MR Z-spectroscopy in vivo: a review of theoretical approaches and methods," Phys Med Biol 58, R221-269 (2013).